Published in final edited form as:

Nat Chem. 2010 December ; 2(12): 1050–1055. doi:10.1038/nchem.890.

Synergistic self-assembly of RNA and DNA molecules

Seung Hyeon Ko[1], **Min Su**[2], **Chuan Zhang**[1], **Alexander E. Ribbe**[1], **Wen Jiang**[2], and **Chengde Mao**[1,*]

[1]Department of Chemistry, Purdue University, West Lafayette, Indiana 47907, USA

[2]Markey Center for Structural Biology and Department of Biological Sciences, Purdue University, West Lafayette, Indiana 47907, USA

Abstract

DNA has recently been used as a programmable 'smart' building block for the assembly of a wide range of nanostructures. It remains difficult, however, to construct DNA assemblies that are also functional. Incorporating RNA is a promising strategy to circumvent this issue as RNA is structurally related to DNA but exhibits rich chemical, structural and functional diversities. However, only a few examples of rationally designed RNA structures have been reported. Herein, we describe a simple, general strategy for the *de novo* design of nanostructures in which the self-assembly of RNA strands is programmed by DNA strands. To demonstrate the versatility of this approach, we have designed and constructed three different RNA–DNA hybrid branched nanomotifs (tiles), which readily assemble into one-dimensional nanofibres, extended two-dimensional arrays and a discrete three-dimensional object. The current strategy could enable the integration of the precise programmability of DNA with the rich functionality of RNA.

Molecular self-assembly holds promise as an effective approach for nanoconstruction[1–4]. The use of DNA, in particular, has been extensively explored as smart building blocks[5–9]. This has led to the successful assembly of many well-defined nanostructures[10–27], but the question remains of how to prepare functional DNA assemblies. RNA, in contrast, exhibits rich chemical, structural and functional diversities. For example, mRNAs carry information that directs protein syntheses, and rRNAs fold and assemble into ribosomes. Ribozymes catalyse chemical reactions, aptamers can specifically bind to ligands, and microRNAs and siRNAs regulate gene activities. If RNA could be used as building blocks for nanoconstruction, it would be straightforward to incorporate naturally existing structural and functional RNA modalities into self-assembled nanostructures. However, the rational design and assembly of RNA architectures remains a challenge. Only a few examples have been

*Correspondence and requests for materials should be addressed to C.M. mao@purdue.edu.

Author contributions: S.H.K. and C.Z. prepared samples and gel analysis. S.H.K. and A.E.R. performed AFM and DLS analysis. M.S., C.Z. and W.J. performed cryoEM imaging and three-dimensional reconstruction. All authors analysed the data and wrote the manuscript. C.M. directed the study.

The authors declare no competing financial interests.

Supplementary information accompanies this paper at www.nature.com/naturechemistry.

reported[28–32], and these are primarily based on naturally existing RNA structural motifs. It is highly desirable to develop rational and versatile strategies for the self-assembly of nanostructures that can integrate RNA molecules. We report a general and remarkably simple strategy for *de novo* design of RNA-containing nanostructures where RNA self-assembly is programmed by DNA molecules.

The strategy relies on synergistic self-assembly of RNA and DNA. RNA strands are guided by DNA strands to self-assemble into hybrid RNA–DNA branched motifs. RNA and DNA can recognize each other according to Watson–Crick base-pairing (A–T/U and G–C) and form RNA–DNA hetero-duplexes. Based on the structural similarity of RNA and DNA, we hypothesize that single-stranded RNA and DNA molecules can be programmed to self-assemble into well-defined RNA–DNA hybrid nanomotifs. DNA motifs that have previously been well characterized, such as double crossovers (DX)[11], three-point stars[33] and four-point stars[12,34], can be adapted into RNA–DNA hybrid motifs. We anticipate that the hybrid motifs behave similarly to their DNA counterparts and can self-assemble into large, extended or discrete structures. Both the homo-DNA duplex (B-form) and the hybrid RNA–DNA duplex (A-form) are right-handed, but they are different in many ways. In the current study, we adjusted the repeating lengths of the duplexes from 10.5 base pairs/turn (bp/turn) for the homo-DNA duplexes to 11 bp/turn for the hybrid RNA–DNA duplexes. To reduce the heterogeneity and increase the structural predictability of the nanomotifs, each helical domain in our design consists of an RNA strand and a complementary DNA strand. In all the structures, all duplexes are A-form RNA–DNA hetero-duplexes.

Results

We first tested the proposed strategy by designing a symmetric RNA–DNA hybrid DX motif (Fig. 1) to assemble extended two-dimensional arrays. In this motif, there are two parallel hetero-duplexes that are joined together at two points where strands cross over from one duplex to the other. The DX motif is composed of five nucleic acid strands: one central, long, two times repetitive DNA strand (**L2**), two identical, short, peripheral DNA strands (**S**) and two RNA strands (**R**). Although strands **L** and **S** cross between duplexes, each **R** strand continuously extends through one duplex from one end to the other. A twofold rotational axis passes through the centre of the motif and is perpendicular to the tile plane. Because of this symmetry, the two **S** strands are identical, as are the two **R** strands.

Each DX tile only needs three unique, component strands: **L**, **R** and **S**. Strand **R** is an RNA molecule, and strands **L** and **S** are both DNA molecules. This design ensures that all helical domains are hetero-RNA–DNA duplexes. The DX tiles have single-stranded overhangs (sticky ends) at each end of the two duplexes. Two neighbouring DX tiles can then associate with each other through hybridization of these sticky ends. The distance between the two crossover points in the tile is set as two turns (22 bp). To allow the DX tiles to tessellate a plane instead of forming one-dimensional arrays, it is essential to keep any two adjacent, interacting DX tiles coplanar, which requires the distance between the two adjacent crossover points of two interacting DX tiles to be $n + 0.5$ turns (n is an integer). In the current design, we set this distance at 2.5 turns (29 bp).

The self-assembly of RNA–DNA hybrid nanostructures is a one-pot process. An aqueous-solution mixture of the component DNA and RNA strands at the designated ratio is slowly cooled from 70 °C to 25 °C over 24 h. In the process, the DNA–RNA strands recognize and associate with each other, first into individual DX tiles and then into large assemblies. The assemblies were analysed by native polyacrylamide gel electrophoresis (PAGE) and visualized by atomic force microscopy (AFM). In native PAGE (Supplementary Fig. S2), all DNA–RNA complexes appeared as sharp bands with the expected mobility, indicating that the hybrid complexes were formed and stable. For AFM imaging, the samples were deposited onto mica surfaces. Large two-dimensional crystals and tubular structures were clearly visible (Fig. 1; Supplementary Fig. S3). The apparent height of the single-layered two-dimensional crystals was 2.1 nm, a reasonable value for the diameter (2.5 nm) of A-form duplexes as RNA–DNA duplexes would deform upon being absorbed onto mica surfaces. The two-dimensional crystals showed clear periodicities both along and perpendicular to their helical axes.

The distance between two adjacent crossover points of two interacting DX tiles (2.5 turns or 29 bp, as indicated in Fig. 1b, inset) is important for ensuring that all DX tiles are coplanar in the final assemblies. If this distance deviates from this value, the helical nature of the duplexes would cause any two interacting tiles to be on different planes, and promote the formation of tubular structures. When this distance is decreased by 1 or 2 bp from 29 bp, the hybrid DX tiles are still able to assemble into large structures, which are predominantly tubular (their heights are much higher than 2.5 nm, the diameter of an A-form duplex), and sometimes extended two-dimensional crystals. The tubular structures are occasionally ripped into monolayers, the regular patterns of which can be observed. When the distance increases by 1 bp or decreases by 3 bp, the hybrid DX tiles do not form any large, regular assemblies. Overall, the formation of tubules is preferred over two-dimensional arrays in all cases, and RNA–DNA hybrid DX tiles are more prone than pure DNA DX tiles to form tubular structures.

The strategy of using DNA to program RNA self-assembly is a general approach and can be used for the construction of a variety of structures. To demonstrate this capability, we engineered two RNA–DNA hybrid star motifs. Symmetric DNA star motifs are a family of related nanostructures that have different numbers of branches (3, 4, 5 and 6). The rotational symmetry axes pass through the tile centres and relate the component branches. Each motif is assembled from three different strands: a long repetitive strand (**L**), a medium strand (**M**) and a short peripheral strand (**S**). All star motifs share the same strands **M** and **S**, but differ from one another in strand **L**. The sequence repeating time of the **L** strand determines the branch number of the motif.

In the current work, the **M** strand is replaced by an RNA strand (**R**), resulting in RNA–DNA hybrid star motifs. RNA residues comprise half of the nanomotifs. When appropriate sticky ends are present at the peripheral ends of the duplexes, the hybrid motifs can further associate with each other into two-dimensional arrays (Figs 2 and 3). The **L** strands contain unpaired, single-stranded loops (shown in orange in Figs 2 and 3; three or four bases long for the three- or four-pointed star, respectively) at the centre. The short loops are long enough to prevent the branches from stacking with one another at the centre, and short

enough to prevent the tiles from being too flexible. To prevent the intrinsic curvatures of the tiles from accumulating in one direction, a corrugation strategy was also applied[12,33,34]. Any two interacting tiles are separated by 4.5 turns, so the two adjacent tiles are related by a twofold rotational axis that is perpendicular to the molecular plane. This arrangement cancels the intrinsic curvatures of the tiles and promotes the tiles to form extended two-dimensional arrays.

During slow cooling, the RNA–DNA hybrid star tiles readily assemble into two-dimensional crystals, which can be visualized by means of AFM imaging. The four-point star tiles assemble into periodic two-dimensional arrays (Fig. 2) with an apparent height of ∼2.2 nm. The cavities in the resulting two-dimensional crystals, to our surprise, are not squares. Instead, they have rectangular shapes. Their dimensions are (27.2 ± 1.6 nm) × (19 ± 1.4 nm). This observation suggests that the overall geometry of the individual RNA–DNA hybrid tile is a skewed four-point star or a four-leafed pinwheel (Fig. 2f). Any two opposite leafs of the hybrid star are shifted away by 4 nm from one another in the direction perpendicular to the helical axes. The overall tile structure is quite different from that of its homo-DNA counterpart. It is unlikely that this is due to a surface phenomenon of differential adsorption onto the mica substrate. The two faces of the two-dimensional arrays are identical to each other, as many twofold rotational symmetry axes (for example, the twofold rotational axes indicated by the bold black arrows shown in Figs 2b and 3b) exist in the plane. A similar phenomenon, although less obvious, can be observed for the RNA–DNA hybrid three-point star motif (Fig. 3). Its overall geometry is a skewed three-point star or three-leafed pinwheel with a threefold rotational symmetry. Consequently, two-dimensional arrays of such tiles only have threefold, instead of sixfold, rotational symmetries. The cavities in the two-dimensional arrays are not regular hexagons. They have alternating long and short sides.

The strategy of DNA-programmed RNA self-assembly is not limited to two-dimensional self-assembly; it can also be applied to three-dimensional self-assembly. To demonstrate the three-dimensional assembly, we assembled an RNA–DNA hybrid dodecahedron based on the hybrid three-point star motif (Fig. 4). A dodecahedron consists of 20 vertices, 12 pentagon faces and 30 edges. Each vertex has a connectivity of 3 and can be represented by a three-point star tile. The hybrid three-point star is similar to the one used for assembling trigonal two-dimensional arrays. However, the three-point star tiles in dodecahedra are significantly bent away from a planar structure. To provide enough flexibility for the tile to bend, the central single-stranded loops on the **L** strand are elongated from 3 to 11 bases. In addition, any two interacting tiles are designed to be separated by four turns (an integral number of turns). At such a separation, any two interacting tiles will face the same side of the tile plane, and any intrinsic tile curvatures will accumulate in the same direction. In turn, this will promote the tiles to assemble into closed, discrete structures[17].

Similarly to two-dimensional self-assembly, the assembly process for three-dimensional structures is a simple one-pot process. Self-assembled RNA–DNA hybrid dodecahedra have been characterized by dynamic light scattering (DLS) and cryogenic electron microscopy (cryoEM) imaging. The hydrodynamic radius of the hybrid complex is 20.7 ± 1.3 nm as measured by DLS. The value is consistent with the radius (20.5 nm) of the circumscribed sphere of the hybrid dodecahedron model, assuming a pitch of 0.26 nm/bp and a diameter of

2.3 nm for the RNA–DNA hetero-duplex. CryoEM allows direct visualization of the hybrid dodecahedral structure (Fig. 4). In the raw images, randomly distributed dodecahedral particles are observed, which are of the expected size. Some small fragments and large aggregates also exist—it is not clear whether those undesired structures are formed during the assembly process or result from damage accompanying sample preparation. The yield of the correctly formed particle is ∼40%, based on visual observation of the cryoEM images (this is significantly lower than the assembly yield of pure DNA dodecahedrons).

From the experimentally observed particles, a three-dimensional map of the RNA–DNA hybrid dodecahedron is generated by single-particle three-dimensional reconstruction, a powerful technique routinely used by structural virologists[35]. The map resolution was determined to be at 2.5 nm using the Fourier shell correlation (0.5 threshold criterion) of two three-dimensional maps independently built from half data sets. There is clear similarity between the computer-generated two-dimensional projections from the reconstructed structural model and the raw, individual particle images (Fig. 4e), and the class averages of raw particle images with similar views (Supplementary Fig. S7). Such comparisons confirm that the reconstructed model is reliable. The radius of the reconstructed dodecahedron model is 20.5 nm, consistent with both the design and the DLS data. The skewness of the star motif is not observed from the reconstructed structural model, as it was in the two-dimensional arrays, presumably due to the low resolution of our cryoEM data.

Discussion

When considering which strand of the overall assembly should be RNA, our guideline was to make sure that every helical domain was composed of one DNA strand and one RNA strand. This ensures that all helical domains will be uniform, hybrid A-form duplexes. Such homogeneity minimizes the occurrence of undesired structural variations in this initial study. Based on this reasoning, we chose RNA as the constituent for the ‘red strands’ in the tiles, but not for the green or black strands (according to the colour code of the figures). Theoretically, it is also possible to simultaneously use RNA for the green and black strands and DNA only for the red strand. It is also possible to use RNA only for all three strands (green, red and black). However, we have not experimentally explored this possibility, and it is not our intention, either. In general, RNA strands are more difficult to prepare, much less stable, and much more expensive than DNA strands with exactly the same sequence. Thus, we decided to use the minimum number (here only one) of RNA strands in the current study.

For two-dimensional self-assembly of star motifs of either homo-DNA or RNA–DNA hybrid, the symmetry remains the same: three- or fourfold rotational symmetry (Figs 2 and 3). In the design of the star motifs, each branch is an identical crossover structure and three- or fourfold rotational symmetries are expected. In the previous homo-DNA structures, the star motif exhibits near D3 or D4 symmetry. Those higher-degree symmetries are a surprising finding, and not the results expected from the design. The different appearance of the star motifs for homo-DNA and hybrid RNA–DNA structures is likely due to the subtle difference between A- and B-form duplexes at the central region of the tile (Supplementary Fig. S6). For a B-form duplex, the base pairs stack directly onto one another and go through the centre of the DNA helix. In contrast, base pairs in an A-form duplex are shifted from one

another, and a cavity appears in the centre of the duplex when looking down the duplex. The base pairs do not go through the centre of the duplex. In addition, the negative charges on the phosphate groups are distributed differently along the different forms of the duplexes. Electrostatic interactions would affect the homo- or hybrid duplexes differently, causing a structural adjustment to minimize the electrostatic repulsion.

Originally, we intended to assemble an RNA–DNA hybrid tetrahedron. Single-stranded loops (11 bases long; the orange segments in strand **L3**) were used at the centre to provide enough flexibility for the motif to bend, but a dodecahedron formed instead of a tetrahedron. This observation suggests that the RNA–DNA hybrid star motifs are more rigid than their corresponding homo-DNA star motifs.

Some fundamental differences exist between pure DNA nanostructures and hybrid RNA–DNA nanostructures. The most important challenge for RNA self-assembly is to rationally design and construct well-defined, stiff, branching motifs, the basic building blocks for nanoconstruction. To appreciate the level of challenge, it is worth giving one example. In the presence of divalent cations, a four-arm DNA junction always adopts a right-handed, X-shaped structure. However, a four-arm RNA–DNA hybrid junction can be either right- or left-handed[36,37]. Compared with this challenge, it is simple and straightforward to adjust the repeating length for the different duplex forms. In the present study, we have also observed numerous different behaviours of the A- and B-form duplexes in nanoconstruction, including the strong tendency of hybrid DX to form tubular structures, the skewed appearance of the star motifs, and the surprising three-dimensional assembly results. Further studies are clearly needed to fully establish the rules for RNA nanoengineering.

There are also some predictable differences between RNA and DNA. Thermodynamically, RNA–DNA hybrid complexes are more stable than homo-DNA complexes. For example, star motifs (with four-base-long sticky ends) associate with one another and form low-mobility, high-molecular-weight species (smears) in the absence of divalent cations (Supplementary Fig. S5). In contrast, under the same conditions, the corresponding homo-DNA motifs will not associate with each other. However, RNA–DNA hybrid structures in the current study were chemically less stable than the corresponding homo-DNA structures. For example, homo-DNA structures do not change noticeably under AFM imaging after being stored for one week at 4 °C, but the RNA–DNA hybrid structures will degrade, and no well-defined nanoarray can be found under AFM imaging after such storage.

As well as the current approach for introducing RNA into DNA nanostructures, a more straightforward method is simply to create DNA nanostructures with appended, single-stranded oligonucleotides with which RNA strands can hybridize. However, the joints between the DNA scaffolds and the RNA moieties are flexible. Such flexibility reduces structural control. Furthermore, the RNA moieties will be fully accessible to the surrounding solvent, harsh chemicals and degrading enzymes (RNases), and are therefore prone to degradation. With the strategy reported here, it is possible to tightly fold RNA deep inside the nanostructures to prevent such RNase accessibility (this is in our study plan). In summary, they are two complementary strategies that each might be appropriate for different applications.

Conclusions

The presented strategy of using DNA to program RNA self-assembly comprises a versatile method for assembling RNA molecules into a range of nanostructures. We believe that this strategy can be applied to all established DNA nanomotifs and DNA origami. Some unexpected phenomena (such as the fact that the star motifs are not straight) have also emerged. To fully understand such phenomena and achieve tight structural controls, a systematic, theoretical modelling and experimental studies are necessary. We expect this strategy to provide a unified platform for assembling both RNA and DNA into large nanostructures with multifunctional RNA modalities: siRNAs, microRNAs, antisense RNAs, ribozymes and aptamers. Currently, we are actively investigating this strategy for fabricating hybrid RNA–DNA nanoparticles for cellular deliveries of small RNAs: aptamers for cellular targeting and other small RNA–DNAs for gene regulation.

Methods

Oligonucleotides, formation of RNA–DNA complexes and imaging

RNA molecules were transcribed with T7 RNA polymerase from the corresponding DNA templates, which were designed by the SEQUIN[38] computer program and purified with PAGE. To form the designed nanostructures, RNA and DNA strands were combined according to the correct molecular ratios in a Tris–acetic–EDTA–Mg^{2+} (TAE/Mg^{2+}) buffer and slowly cooled from 70 °C to room temperature. After annealing, the samples were visualized by tapping-mode AFM on a Multimode AFM with Nanoscope IIIa controller (Veeco) in air at 22 °C. For cryoEM Imaging, RNA–DNA sample solutions were concentrated to ∼3 μM, spread onto Quantifoil grids, then plunge-frozen. Data were recorded using a Gatan 4k × 4k charge-coupled device (CCD) camera in a Philips CM200 transmission electron microscope.

Single particle reconstruction

Three-dimensional reconstructions of the DNA dodecahedra used the single-particle image-processing software EMAN[39]. An icosahedral symmetry for the polyhedra was established by processing the images assuming different symmetries and finding the symmetry that yielded a three-dimensional reconstruction consistent with the particle images. Final three-dimensional maps were visualized using UCSF Chimera software[40].

Supplementary Material

Refer to Web version on PubMed Central for supplementary material.

Acknowledgments

This work was supported by the Office of Naval Research, the National Institutes of Health and a Lilly Seed grant through Purdue University. AFM and DLS studies were carried out in the Purdue Laboratory for Chemical Nanotechnology (PLCN). The cryoEM images were taken in the Purdue Biological Electron Microscopy Facility and the Purdue Rosen Center for Advanced Computing (RCAC) provided the computational resource for the three-dimensional reconstructions.

References

1. Whitesides GM, Mathias JP, Seto CT. Molecular self-assembly and nanochemistry: a chemical strategy for the synthesis of nanostructures. Science. 1991; 254:1312–1319. [PubMed: 1962191]
2. Hamley IW. Nanotechnology with soft materials. Angew Chem Int Ed. 2003; 42:1692–1712.
3. Lehn JM. Toward complex matter: Supramolecular chemistry and self-organization. Proc Natl Acad Sci USA. 2002; 99:4763–4768. [PubMed: 11929970]
4. Reinhoudt DN, Crego-Calama M. Synthesis beyond the molecule. Science. 2002; 295:2403–2407. [PubMed: 11923525]
5. Seeman NC. DNA in a material world. Nature. 2003; 421:427–431. [PubMed: 12540916]
6. Lin C, Liu Y, Rinker S, Yan H. DNA tile based self-assembly: building complex nano-architectures. ChemPhysChem. 2006; 7:1641–1647. [PubMed: 16832805]
7. Feldkamp U, Niemeyer CM. Rational design of DNA nanoarchitectures. Angew Chem Int Ed. 2006; 45:1856–1876.
8. Aldaye FA, Palmer AL, Sleiman HF. Assembling materials with DNA as the guide. Science. 2008; 321:1795–1799. [PubMed: 18818351]
9. Simmel FC. Three-dimensional nanoconstruction with DNA. Angew Chem Int Ed. 2008; 47:5884–5887.
10. Chen JH, Seeman NC. Synthesis from DNA of a molecule with the connectivity of a cube. Nature. 1991; 350:631–633. [PubMed: 2017259]
11. Winfree E, Liu FR, Wenzler LA, Seeman NC. Design and self-assembly of two-dimensional DNA crystals. Nature. 1998; 394:539–544. [PubMed: 9707114]
12. Yan H, Park SH, Finkelstein G, Reif JH, LaBean TH. DNA-templated self-assembly of protein arrays and highly conductive nanowires. Science. 2003; 301:1882–1884. [PubMed: 14512621]
13. Shih MW, Quispe JD, Joyce GF. A 1.7-kilobase single-stranded DNA that folds into a nanoscale octahedron. Nature. 2004; 427:618–621. [PubMed: 14961116]
14. Rothemund PWK, Papadakis N, Winfree E. Algorithmic self-assembly of DNA Sierpinski triangles. PLoS Biol. 2004; 2:2041–2053.
15. Goodman RP, et al. Rapid chiral assembly of rigid DNA building blocks for molecular nanofabrication. Science. 2005; 310:1661–1665. [PubMed: 16339440]
16. Rothemund PWK. Folding DNA to create nanoscale shapes and patterns. Nature. 2006; 440:297–302. [PubMed: 16541064]
17. He Y, et al. Hierarchical self-assembly of DNA into symmetric supramolecular polyhedra. Nature. 2008; 452:198–201. [PubMed: 18337818]
18. Yin P, Choi HM, Calvert CR, Pierce NA. Programming biomolecular self-assembly pathways. Nature. 2008; 451:318–322. [PubMed: 18202654]
19. Yin P, et al. Programming DNA tube circumferences. Science. 2008; 321:824–826. [PubMed: 18687961]
20. Andersen ES, et al. Self-assembly of a nanoscale DNA box with a controllable lid. Nature. 2009; 459:73–76. [PubMed: 19424153]
21. Douglas SM, et al. Self-assembly of DNA into nanoscale three-dimensional shapes. Nature. 2009; 459:414–418. [PubMed: 19458720]
22. Dietz H, Douglas SM, Shih WM. Folding DNA into twisted and curved nanoscale shapes. Science. 2009; 325:725–730. [PubMed: 19661424]
23. Alivisatos AP, et al. Organization of ‘nanocrystal molecules’ using DNA. Nature. 1996; 382:609–611. [PubMed: 8757130]
24. Park SY, et al. DNA-programmable nanoparticle crystallization. Nature. 2008; 451:553–556. [PubMed: 18235497]
25. Nykypanchuk D, Maye MM, van der Lelie D, Gang O. DNA-guided crystallization of colloidal nanoparticles. Nature. 2008; 451:549–552. [PubMed: 18235496]
26. Sharma J, et al. Control of self-assembly of DNA tubules through integration of gold nanoparticles. Science. 2009; 323:112–116. [PubMed: 19119229]

27. Li Y, et al. Enzyme-catalysed assembly of DNA hydrogel. Nature Mater. 2004; 3:38–42. [PubMed: 14704783]
28. Jaeger L, Leontis NB. Tecto-RNA: one-dimensional self-assembly through tertiary interactions. Angew Chem Int Ed. 2000; 39:2521–2524.
29. Chworos A, et al. Building programmable jigsaw puzzles with RNA. Science. 2004; 306:2068–2072. [PubMed: 15604402]
30. Severcan I, Geary C, Verzemnieks E, Chworos A, Jaeger L. Square-shaped RNA particles from different RNA folds. Nano Lett. 2009; 9:1270–1277. [PubMed: 19239258]
31. Shu D, Moll D, Deng Z, Mao C, Guo P. Bottom-up assembly of RNA arrays and superstructures as potential parts in nanotechnology. Nano Lett. 2004; 4:1717–1723. [PubMed: 21171616]
32. Afonin KA, Cieply DJ, Leontis NB. RNA self-assembly with minimal paranemic motifs. J Am Chem Soc. 2008; 130:93–102. [PubMed: 18072767]
33. He Y, Chen Y, Liu H, Ribbe AE, Mao C. Self-assembly of hexagonal DNA two-dimensional (2D) arrays. J Am Chem Soc. 2005; 127:12202–12203. [PubMed: 16131180]
34. He Y, et al. Sequence symmetry as a tool for designing DNA nanostructures. Angew Chem Int Ed. 2005; 44:6694–6696.
35. Jiang W, et al. Backbone structure of the infectious ε15 virus capsid revealed by electron cryomicroscopy. Nature. 2008; 451:1130–1134. [PubMed: 18305544]
36. Nowakowski J, Shim PJ, Stout CD, Joyce GF. Alternative conformation of a nucleic acid four-way junction. J Mol Biol. 2000; 300:93–102. [PubMed: 10864501]
37. Nowakowski J, Shim PJ, Prasad GS, Stout CD, Joyce GF. Crystal structure of an 82-nucleotide RNA–DNA complex formed by the 10–23 DNA enzyme. Nature Struct Biol. 1999; 6:151–156. [PubMed: 10048927]
38. Seeman NC. De novo design of sequences for nucleic acid structure engineering. J Biomol Struct Dyn. 1990; 8:573–581. [PubMed: 2100519]
39. Ludtke SJ, Baldwin PR, Chiu W. EMAN: semiautomated software for high-resolution single-particle reconstructions. J Struct Biol. 1999; 128:82–97. [PubMed: 10600563]
40. Goddard TD, Huang CC, Ferrin TE. Visualizing density maps with UCSF Chimera. J Struct Biol. 2007; 157:281–287. [PubMed: 16963278]

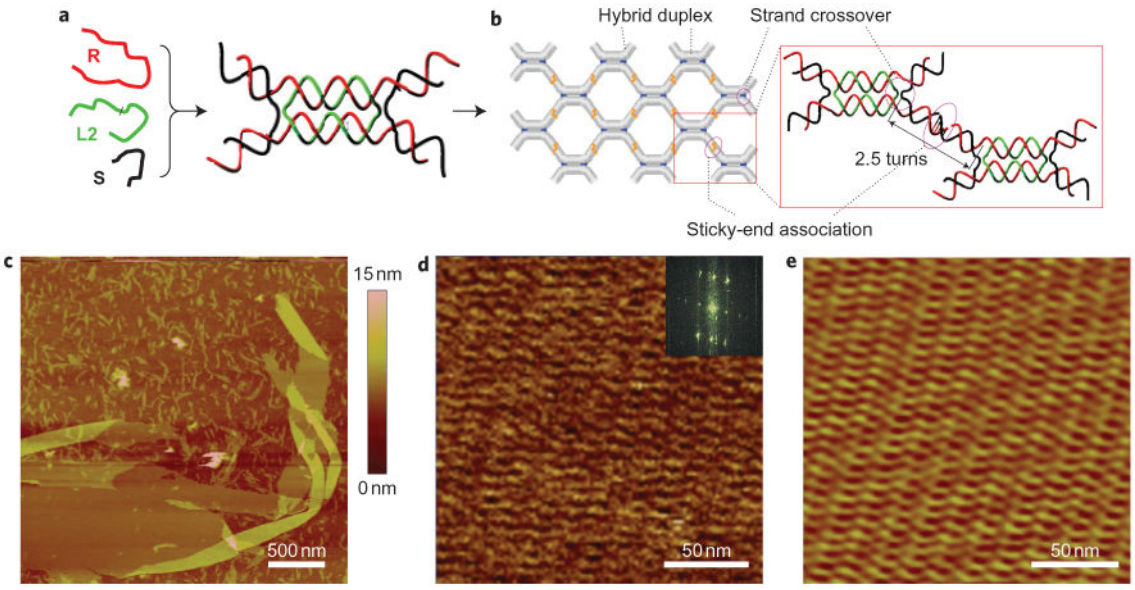

Figure 1. DNA-programmed RNA self-assembly: an RNA–DNA hybrid double crossover (DX) motif (tile)

a,b, Individual RNA and DNA strands self-assemble into hybrid DX tiles (**a**) and then further assemble into extended two-dimensional arrays during slow cooling (**b**). In **a** the hybrid DX motif consists of two identical RNA strands (**R**, red), two identical short DNA strands (**S**, black), and a long two-times repetitive DNA strand (**L2**, green). All duplexes are hetero-duplexes, each consisting of an RNA strand and a DNA strand. The four duplex ends have single-stranded overhangs (sticky ends). In **b**, extended two-dimensional DX arrays are formed through sticky-end hybridization among the tiles. Grey tubes, blue dots and staggered orange lines represent hybrid duplexes, locations of strand crossovers between duplexes and sticky-end associations, respectively. The inset on the right shows a detailed view of two associating DX tiles, in which the base-pairing between the sticky ends is shown as thin lines. The locations of both the strand crossover and sticky-end hybridization are circled in purple. **c,d**, AFM images (at different magnifications) of the extended two-dimensional arrays of hybrid DX tiles. The height scale bar is shown adjacent to **c**. The inset in **d** is the corresponding Fourier transform pattern. **e**, Reconstructed pattern of **d** through Fourier transformation.

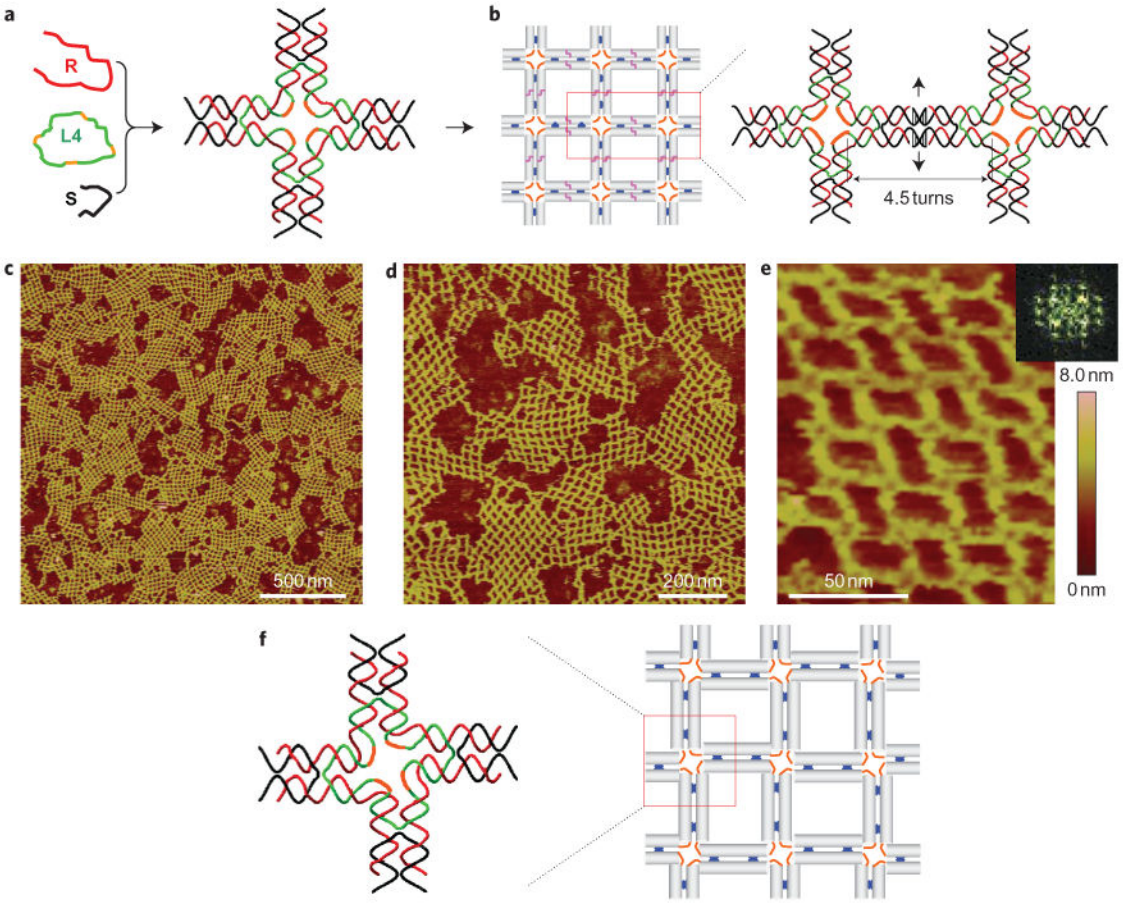

Figure 2. DNA-programmed RNA self-assembly: an RNA–DNA hybrid four-point star motif

a, The hybrid four-point star motif consists of four identical RNA strands (**R**, red), four identical short DNA strands (**S**, black), and a long four-times repetitive DNA strand (**L4**, green and orange). There are four 4-base-long, single-stranded loops (orange) at the centre of the tile. The loops are important for maintaining the fourfold rotational symmetry of the tile and keeping the tile planar. **b**, Extended tetragonal two-dimensional arrays assembled from the four-point star tiles through sticky-end association (shown in purple). Inset on the right provides a detailed view of two associating tiles, which are related to each other by a twofold rotational axis (indicated by a pair of black thick arrows). The separation between the two tiles is 4.5 helical turns. **c–e**, AFM images (at different magnifications) of the two-dimensional arrays of the hybrid four-point star tile. The two-dimensional arrays exhibit alternating rectangular cavities. A height scale bar is shown on the right. Inset in **e** is a Fourier transform pattern. **f**, Revised structural model for the hybrid four-point star tile based on the AFM data. The tile is skewed as a four-leafed pinwheel, but maintains the fourfold rotational symmetry.

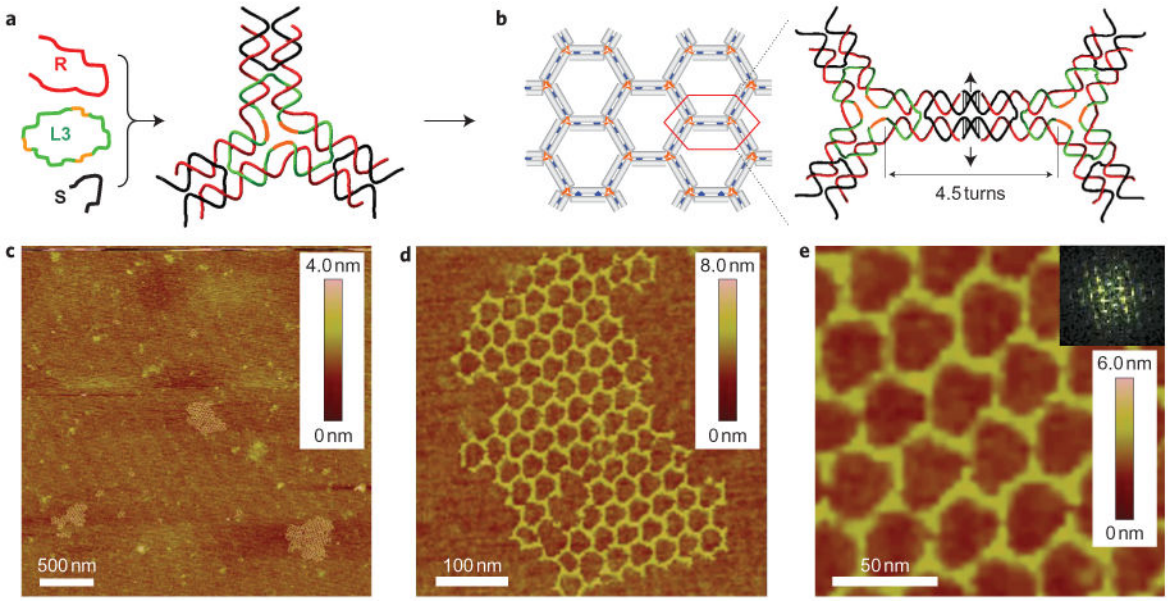

Figure 3. DNA-programmed RNA two-dimensional self-assembly: an RNA–DNA hybrid three-point skewed star motif

a, The hybrid three-point star motif consists of three identical RNA strands (**R**, red), three identical short DNA strands (**S**, black), and a long three-times repetitive DNA strand (**L3**, green and orange). There are three 3-base-long, single-stranded loops (orange) at the centre of the tile. **b**, Extended trigonal two-dimensional arrays assembled from the three-point star tiles through sticky-end association. Inset on the right provides a detailed view of two associating tiles. **c–e**, AFM images (at different magnifications) of the two-dimensional arrays of the hybrid three-point skewed star tile. The two-dimensional arrays exhibit threefold, instead of sixfold, rotational symmetries.

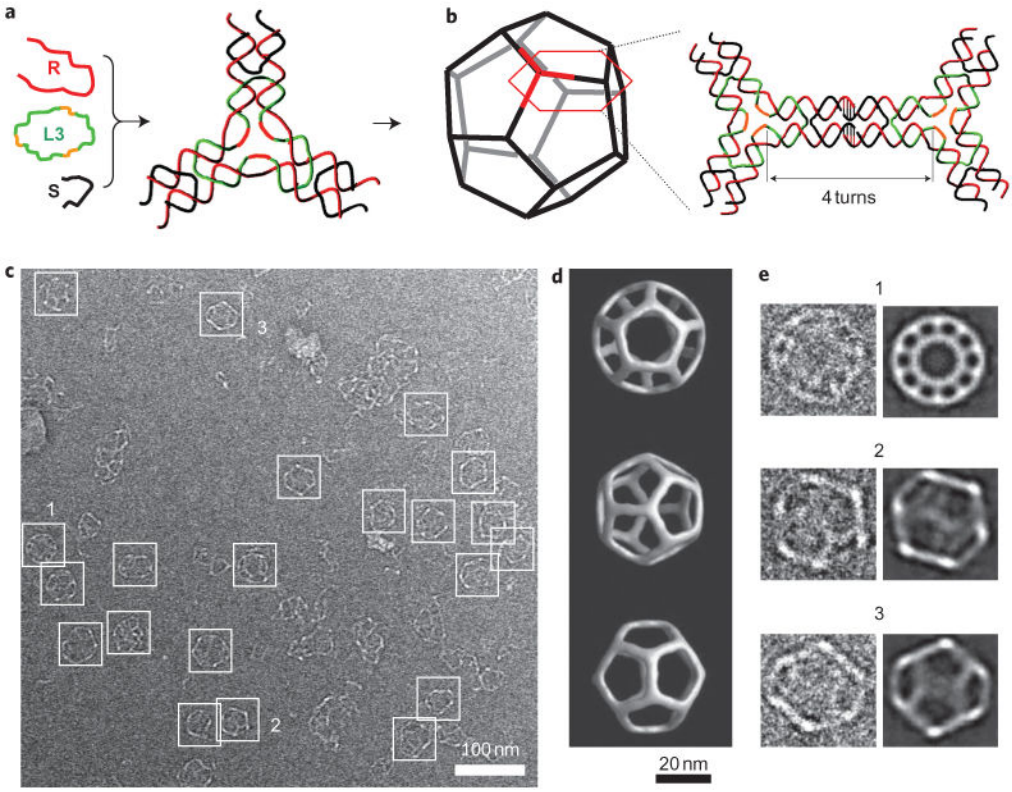

Figure 4. DNA-programmed RNA self-assembly in three dimensions: an RNA–DNA hybrid dodecahedron

a,b, Scheme of the assembly strategy. Note that the distance between two adjacent tiles is four helical turns. **c**, Representative cryoEM image of the RNA–DNA hybrid dodecahedra. White boxes indicate individual hybrid dodecahedral particles. **d**, Three views of the RNA–DNA hybrid dodecahedral structure reconstructed from the cryoEM images. **e**, Raw cryoEM images of individual particles (corresponding to the particles labelled with the same numbers in **c**) and the corresponding projections of the reconstructed dodecahedral structure with similar views.